

Fig. 1 — Schematic diagram of the experimental setup.

indicate that the presence of sulfur may not always lead to a deep weld pool.

What role does the concentration of sulfur play in the case of laser welding? Are the weld pool shape and size truly insensitive to the concentration of sulfur in steels in the case of laser spot welding as indicated in the works of Zacharia, *et al.* (Refs. 16, 17)? The magnitude and direction of the surface-tension-induced shear stress at the weld pool surface is determined by the concentration of surface-active elements, local temperature and its spatial gradient. Therefore, all the factors that affect the weld pool surface temperature distribution must have an influence on the shape and size of the weld pool, cooling rates and weldment properties. In principle, the geometry of the weld pool is determined, in addition to the concentration of surface-active elements, by a combination of various process parameters such as total power, power density, and welding speed. As a result, the concentration of sulfur may

have a pronounced effect under one set of welding conditions, while under a different set of conditions, the effect of sulfur may be completely masked by the dominant effect of one or more of the other welding variables. Without a comprehensive investigation of the effect of all important variables, evaluation of the effect of sulfur, keeping all the other variables constant in all the experiments, may only provide a limited, and, in some instances, misleading answer to the above questions.

The work reported here is aimed at developing a comprehensive understanding of the role of sulfur and processing parameters during conduction mode laser irradiation of steels. We report here the results of an investigation involving more than eighty trials of conduction mode laser spot welds to understand the effects of sulfur concentration, power, power density and irradiation time on the development of weld pool geometry. Furthermore, to understand the experimental results, the effects of these variables are modeled through numerical solution of the equations of conservation of mass, momentum and energy. The computed results are compared with the experimental data to obtain a comprehensive understanding of the role of sulfur concentration, and processing parameters. Both the experimental and theoretical results show that, in the case of conduction mode laser spot welding, changing sulfur concentration may

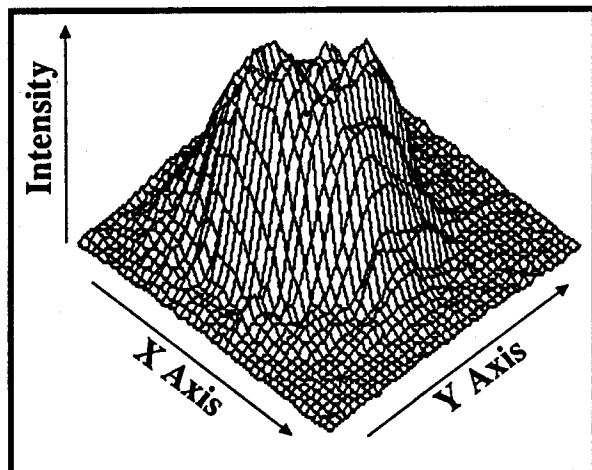


Fig. 2 — The profile of the laser beam used for welding.

or may not have a pronounced effect on the pool shape and size, depending on the processing parameters. It is demonstrated that under certain processing conditions the dimensionless Peclet number, which is the ratio of the rates of convective heat transfer to conductive heat transfer, can have a small value, *i.e.*, lower than one. Under these conditions, the heat is transported primarily by conduction, and the weld pool aspect ratio, defined as the ratio of weld pool depth to width, is not significantly influenced by the sulfur concentration. It is shown that the processing conditions must be controlled carefully to achieve a beneficial aspect ratio in steel welds containing sulfur. For example, at a given laser power and concentration of sulfur, the power density has a strong influence on the temporal evolution of weld pool geometry during multikilowatt conduction mode laser spot welding of steels.

Experimental Procedures

A schematic diagram of the experimental setup is shown in Fig. 1. Spot welds were made using a carbon dioxide laser, manufactured by Trumpf, Germany, Model TLF 6000 turbo, capable of producing a maximum output of 6000 W in the continuous-wave mode. The laser was operated in TEM 01 mode. A focusing mirror with a focal length of 200 mm was used. A typical power density distribution of the beam, measured with an electronic device Laserscope UFF 100, manufactured by Prometec, Germany, is shown in Fig. 2. The power density distribution that reaches the sample surface during the laser-material interaction is expected to be somewhat different from such a measurement, which is due to a slight inclination of the laser beam (10 deg from the vertical), curvature of the weld pool surface, and possibly to gradients in the optical properties of the atmosphere above the weld pool. Special care was taken to prevent any oxygen contamination on the weld pool surface from the atmosphere by shielding the sample with argon, which was passed at a flow rate of 20 L/min from a 10 mm cylindrical nozzle. The spot welding experiments were performed on a computer-controlled workstation capable of controlling laser power, focus position and irradiation time.

Stationary, autogenous welds were made on different heats of Böhler S 705 high-speed steel in the as-cast state. The compositions of the steels are given in Table 1. Plates of approximately 15-mm (0.6-in.) thickness were polished with 800-grit paper and cleaned prior to weld-

Table 1 — Compositions of the Three High-Speed Steels Used in the Investigation

Element	Heat A (wt-%)	Heat B (wt-%)	Heat C (wt-%)
C	0.87	0.88	0.9
Cr	3.89	3.88	3.89
W	6.36	6.33	6.3
Mo	4.87	4.84	4.83
V	1.8	1.79	1.77
Co	4.57	4.56	3.89
Mn	0.24	0.25	0.23
Si	0.53	0.53	0.32
Ti	<0.01	<0.01	<0.005
N	0.032	0.032	0.032
S	0.002	0.015	0.004
Al	<0.005	0.005	0.015
Ca	0.0001	<0.0001	0.0001
O	0.0049	0.0043	0.0035
Fe	balance	balance	balance

ing. Laser irradiation times were far in excess of the typical times for usual spot welding operations. This was necessary to develop a basic understanding of the evolution of the molten pool geometry. Welds were made at a laser power of 5200 W for irradiation times of 0.1, 0.25, 0.5, 0.75, 1, 3, 5, 10 and 15 s to study the temporal evolution of the weld pool geometry. Welds were also made with laser powers of 1900, 3850, and 5200 W for otherwise identical parameters in order to investigate the effect of total power on the weld shape and size. To examine the effect of power density on the weld geometry, different focal distances at a constant power of 5000 W and an irradiation time of 15 s were used to make the welds. To examine the consistency of the results, three welds were made for

most sets of processing conditions. The final geometries of the welds were examined by sectioning the samples along a vertical plane through the center of the welds. The cross-sections of the samples were then examined using standard metallographic procedures and etching with a mixture of ammonium persulfate, ferric chloride and hydrochloric acid with water (Ref. 18).

Mathematical Modeling

A mathematical model, based on the solution of the equations of conservation of mass, momentum and energy in the weld pool, was used to understand the experimental results (Ref. 19). It includes a submodel for the calculation of temperature and composition-dependent surface tension. In the case of spot welding, the pool geometry is assumed symmetrical about the laser beam axis. Therefore, the equations of conservation of mass, momentum and energy were solved in the following transient, two-dimensional axisymmetric form:

Conservation of Mass

$$\frac{\partial \rho}{\partial t} + \frac{1}{r} \frac{\partial}{\partial r} (\rho r u_r) + \frac{\partial}{\partial z} (\rho u_z) = 0 \quad (1)$$

Conservation of Momentum

Radial Direction

$$\rho \frac{\partial u_r}{\partial t} + \rho u_r \frac{\partial u_r}{\partial r} + \rho u_z \frac{\partial u_r}{\partial z} = -\frac{\partial p}{\partial r} - \mu \left\{ \frac{\partial^2 u_r}{\partial r^2} + \frac{\partial^2 u_r}{\partial z^2} + \frac{1}{r} \frac{\partial u_r}{\partial r} - \frac{u_r}{r^2} \right\} \quad (2)$$

Axial Direction

$$\rho \frac{\partial u_z}{\partial t} + \rho u_r \frac{\partial u_z}{\partial r} + \rho u_z \frac{\partial u_z}{\partial z} = -\frac{\partial p}{\partial z} - \mu \left\{ \frac{\partial^2 u_z}{\partial r^2} + \frac{\partial^2 u_z}{\partial z^2} + \frac{1}{r} \frac{\partial u_z}{\partial r} \right\} + \rho g_z \quad (3)$$

Conservation of Enthalpy

$$\rho \frac{\partial \Phi}{\partial t} + \frac{\partial}{\partial z} (\rho u_z \Phi) + \frac{1}{r} \frac{\partial}{\partial r} (\rho u_r \Phi r) = \frac{\partial}{\partial z} \left\{ \frac{k}{c_p} \frac{\partial \Phi}{\partial z} \right\} + \frac{1}{r} \frac{\partial}{\partial r} \left\{ \frac{k}{c_p} r \frac{\partial \Phi}{\partial r} \right\} + S_\Phi(r) \quad (4)$$

where u is the velocity, the subscripts r and z are the radial and the axial direction indicators, respectively, and ρ , μ , p , c_p , k , Φ are the density, viscosity, pressure, specific heat, thermal conductivity and enthalpy, respectively. The symbol $S_\Phi(r)$ is the source of enthalpy and represents the absorption of energy from the laser beam.

In formulating the model, the following assumptions were made:

1) The power density distribution of the laser beam was approximated, for simplicity, by a "top hat" profile based on the experimentally observed profile presented in Fig. 2. A beam radius of 1.4 mm (0.055 in.) was assumed.

2) The fluid flow in the weld pool is driven primarily by the shear stress (Marangoni stress) generated due to spatial variation of surface tension at the weld pool surface.

3) No keyhole formation was observed in the experiments and the surface

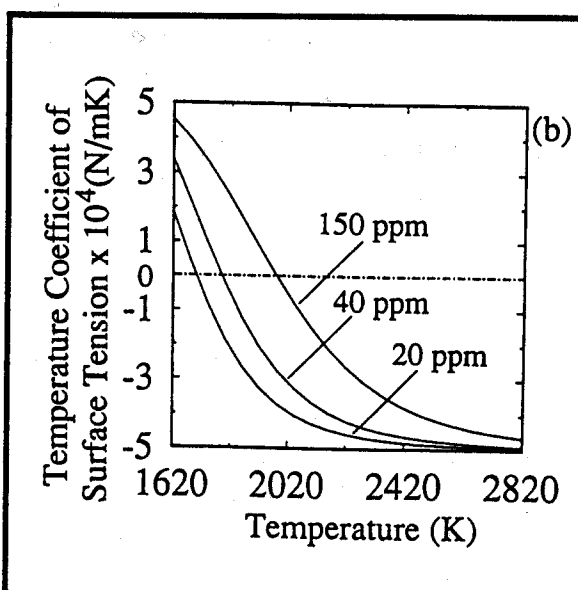
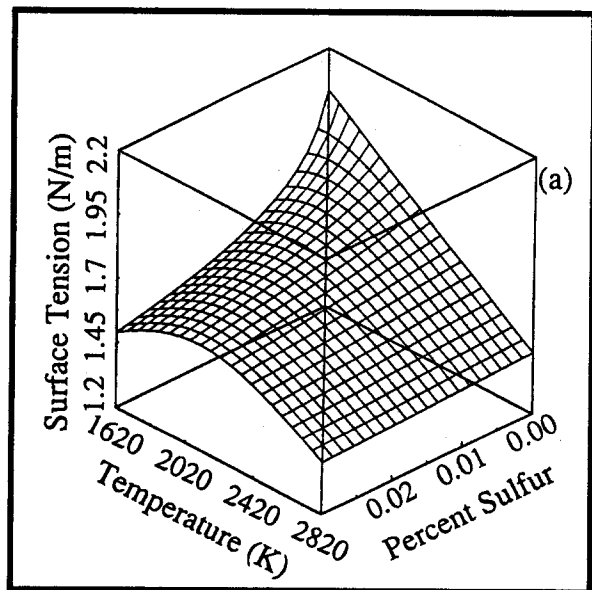


Fig. 3. — Variation of: A — surface tension of Fe-S as a function of temperature and sulfur activity; B — temperature coefficient of surface tension, dy/dT , of Fe-S as a function of temperature for samples containing 20, 40 and 150 ppm sulfur.

RESEARCH DEVELOPMENT RESEARCH DEVELOPMENT RESEARCH DEVELOPMENT

Table 2 — Data Used for the Computation of Surface Tension and Temperature Coefficient of Surface Tension for Fe-S System

Parameter	Value
Melting temperature (K)	1620
Temperature coefficient of surface tension for pure iron, A , (N/m.K)	-5.0×10^{-4}
Surface excess at saturation, Γ_s , (kg-mole/m ²)	1.30×10^{-8}
Entropy factor, k_1	0.00318
Enthalpy of segregation, ΔH^s , (J/kg-mole)	-1.66×10^8

of the weld pool was assumed to be flat.

4) Constant, temperature-independent thermophysical properties were used.

5) The viscosity and the thermal conductivity of the liquid metal in the weld pool were increased from their original values by a constant factor to account for the enhanced heat and mass transport rates resulting from flow of liquid metal in the weld pool.

Since the emphasis of the present work is to investigate the effects of sulfur on the weld pool geometry, it is essential to treat surface tension as a function of temperature and the activity of sulfur. McNallan and DebRoy (Ref. 20) showed that in the 18-8 stainless steel, Ni and Cr concentrations do not significantly affect the value of dy/dT . Based on these results and due to the lack of data for the present alloy system, the theoretical investigations of heat transfer and fluid flow in high-speed steel weld pools were undertaken using a model originally designed to determine the temperature coefficient of surface tension of the Fe-S system (Ref. 21). However, some influence from the other elements, especially from carbon and oxygen, is expected. The model was used to calculate surface tension as a function of temperature and sulfur concentration in the steel. The surface tension as a function of temperature and activity of sulfur is presented in Fig. 3A. The data used for the calculations are pre-

sented in Table 2. The figure shows that the surface tension of the alloy is a strong function of temperature and the sulfur activity. The variation of the temperature coefficient of surface tension as a function of temperature for the steel samples containing 20, 40 and 150 ppm sulfur is given in Fig. 3B. The figure shows a significant difference in dy/dT for the three compositions.

Boundary Conditions

At the surface of the weld pool, the Marangoni effect was incorporated by equating the shear stress to the spatial gradient of surface tension.

$$-\mu \frac{du_r}{dz} = \frac{d\gamma}{dr} = \frac{d\gamma}{dT} \frac{dT}{dr} \quad (5)$$

The top surface also included the prescription of the heat exchange between the surface of the sample and the laser beam.

$$j_\phi(r) = \alpha p_L(r) \quad (6)$$

where $j_\phi(r)$ is the absorbed heat flux density distribution on the surface of the sample, $p_L(r)$ is the laser beam power density distribution and α is the absorption coefficient. In the case of the top-hat laser beam profile, Equation 6 reduces to:

$$j_\phi(r) = \frac{\alpha Q}{\pi r_b^2} \quad \text{for } r \leq r_b \quad (7)$$

where Q is the total laser beam power and r_b is the beam radius.

At the axis of the pool, gradients of enthalpy and axial velocity were taken to be zero on the basis of geometric symmetry. Furthermore, the radial velocity was zero at the axis because of symmetry.

$$\frac{d\Phi}{dr} = 0 \quad (8)$$

$$\frac{du_z}{dr} = 0 \quad (9)$$

$$u_r = 0 \quad (10)$$

At the solid-liquid interface, the curved weld pool boundary was approximated by a series of steps, and the velocities were prescribed to be zero, which amounted to an assumption of no-slip between the liquid and solid surfaces. Similarly, in the solid region the velocities were prescribed to be zero.

$$u_z, u_r = 0 \quad \text{for } \Phi < \Phi_{\text{melt}} \quad (11)$$

where Φ_{melt} is the melting enthalpy.

The sample geometry was chosen to be a disc of 15-mm radius (0.6-in.) and 15-mm thickness. Spatially nonuniform grids were used for maximum resolution of variables. The effect of grid spacings on the computed results was investigated and a grid with 60 cells and a minimum cell size of 0.01 mm in the axial direction and 50 cells and a minimum cell size of 0.1 mm in the radial direction was found to be appropriate. Based on time-step sensitivity studies, the time step in the calculations was chosen to be 0.0001 s for the first 5 s and 0.001 s for the remainder of the irradiation time.

Results and Discussion

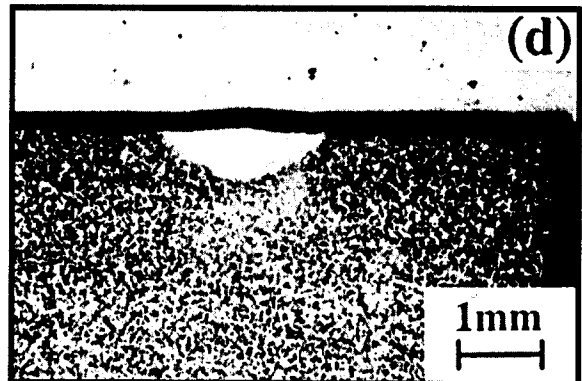
Figure 4A, B and C is the optical micrographs of solidified weld pools of steel samples containing 20 ppm sulfur spot welded for 5 s using 1900-, 3850- and 5200-W laser powers, respectively. All other parameters were kept constant. The focus of the laser beam was positioned 20 mm (0.78 in.) below the sample surface and the spot radius, measured at 5200 W, was approximately 1.4 mm. To examine the effect of sulfur concentration, cross-sections of the welds formed in a steel sample containing 150 ppm of sulfur and welded under identical conditions as the low-sulfur-containing steel are shown in Fig. 4D, E, and F. A comparison of micrographs shows that, at a laser power of 1900 W, the pool geometries were similar in the two steels containing 20 and 150 ppm sulfur. However, when the samples were welded using laser powers of 3850 and 5200 W, the

Table 3 — Data Used for Calculations of Velocity and Temperature Fields

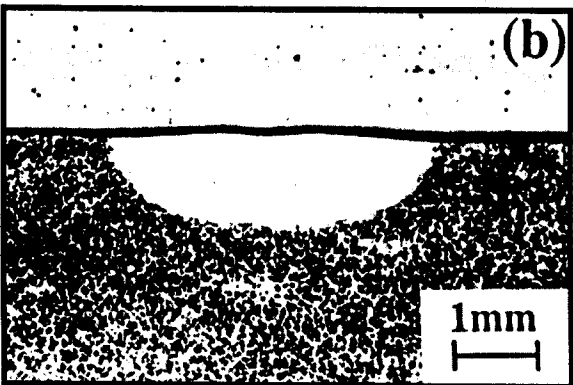
Property/Parameter	Value
Density (kg/m ³)	8100.0
Melting point (K)	1620.0
Viscosity (kg/m-s)	6.0×10^{-3}
Thermal conductivity of solid (J/m-s-K)	22.9
Thermal conductivity of liquid (J/m-s-K)	22.9
Specific heat of solid (J/kg-K)	627.0
Specific heat of liquid (J/kg-K)	723.14
Latent Heat of Melting (J/kg)	250.8×10^3
Viscosity and thermal conductivity enhancement factor	7.0
Argon flow rate (m ³ /s)	3.33×10^{-4}
Absorption coefficient	0.13
Scanning velocity (m/s)	0.0
Beam radius (m)	1.4×10^{-3}

20 ppm Sulfur

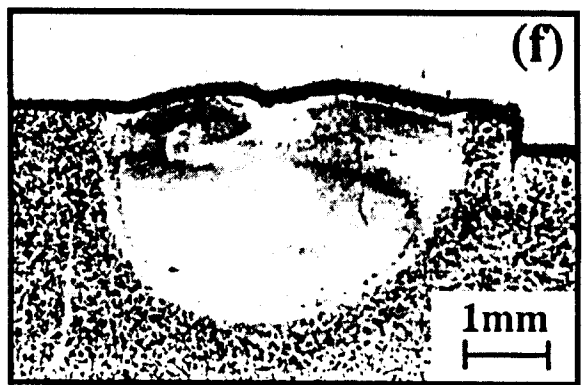
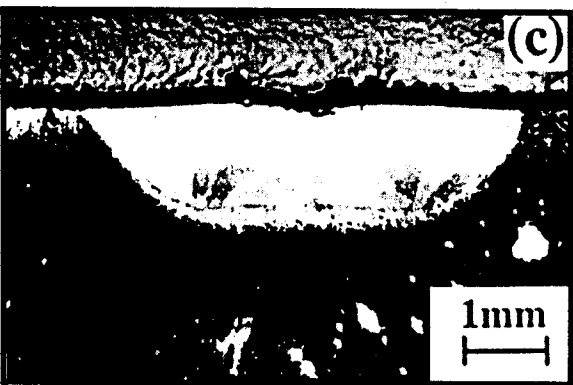
150 ppm Sulfur



1900 W



3850 W



5200 W

Fig. 4 — Optical micrographs of weld geometries for the steel containing 20 ppm sulfur for laser powers of: A — 1900 W; B — 3850 W; C — 5200 W; and for the steel containing 150 ppm sulfur for laser powers of: D — 1900 W; E — 3850 W; F — 5200 W. Irradiation time: 5 s.

weld geometries showed a pronounced dependence on the concentration of sulfur. The welds containing 150 ppm sulfur have much greater depth of penetration than those containing 20 ppm sulfur at high laser powers. Thus, the concentration of sulfur may or may not have a significant effect on the weld geometry depending on the laser power and other

processing parameters when a laser is used as a heat source. The results also demonstrate that the evaluation of the effect of a surface-active element, such as sulfur, using a limited number of experiments, where only the sulfur content is varied and all other parameters are kept constant, can lead to incomplete or misleading conclusions.

Why are the pool shape and size not markedly affected by sulfur concentration at a laser power of 1900 W, whereas sulfur shows a pronounced effect on weld pool geometry at 3850 and 5200 W? Since the weld pool shape and size are determined by a combination of conductive and convective heat transfer, understanding of heat transfer in the weld pool

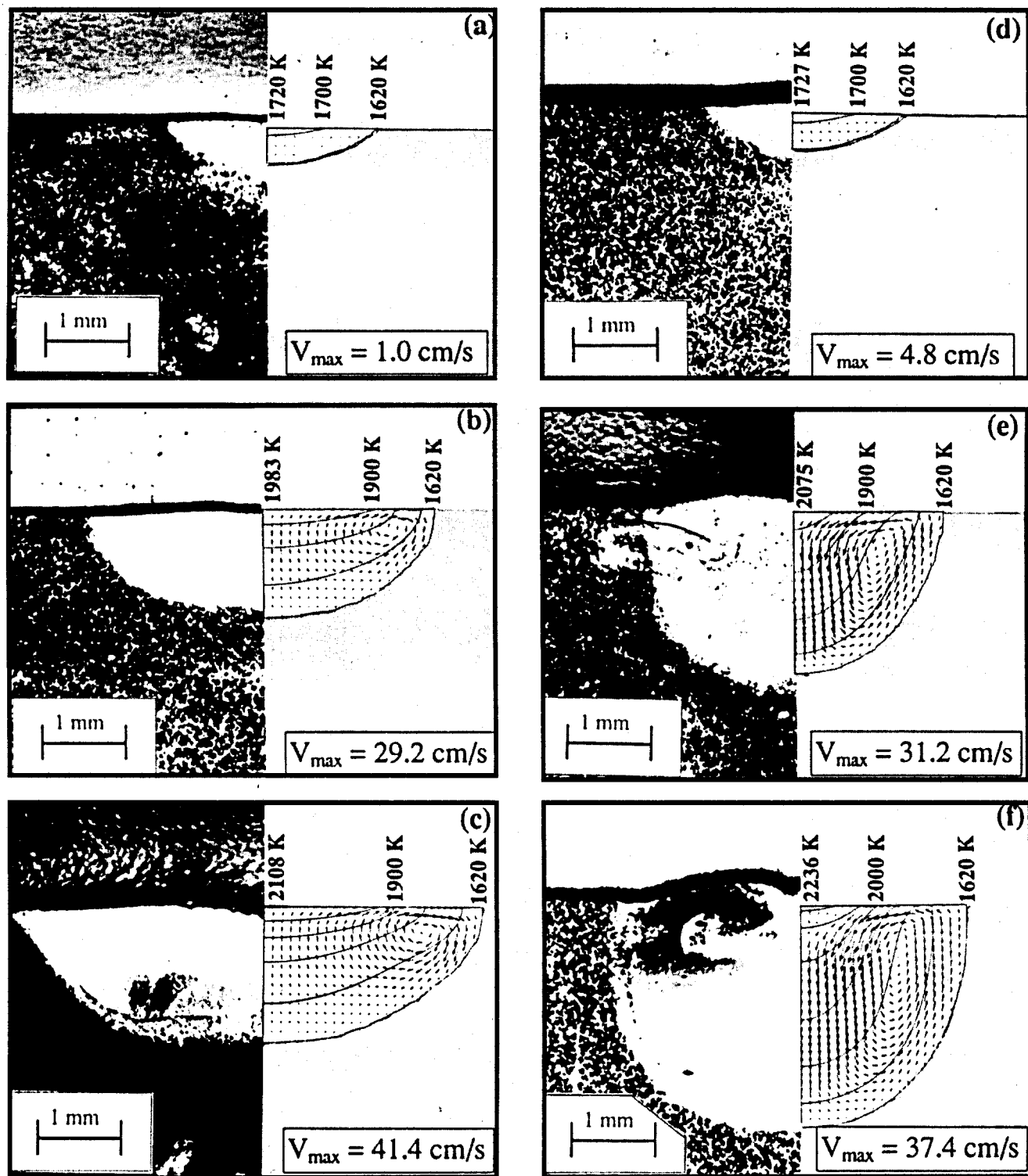


Fig. 5 — Comparison of the predicted weld pool geometries with the experimental observations for the steel containing 20 ppm sulfur for laser powers of: A — 1900 W; B — 3850 W; C — 5200 W; and for the steel containing 150 ppm sulfur for laser powers of: D — 1900 W; E — 3850 W; F — 5200 W. Irradiation time: 5 s.

must be the basis for examining the relative importance of laser power and weld metal sulfur concentration for various processing conditions. Therefore, numerical simulations of heat transfer and fluid flow were carried out to understand the experimental results. The predicted weld geometries for the three powers for an

radiation time of 5 s are compared with the corresponding experimental data in Fig. 5 for samples containing 20 and 150 ppm sulfur. The data used for the calculations are presented in Table 3. It is observed from Fig. 5A and D that for a laser power of 1900 W, there is no significant difference between the computed weld

geometries containing different sulfur concentrations. This insensitivity of weld geometry on sulfur concentration is consistent with the experimental observations. However, for laser powers of 3850 and 5200 W, the predicted geometries in Fig. 5B, C, E and F show that the weld penetration is deeper in the steel with 150

ppm sulfur than in the steel containing 20 ppm sulfur. Furthermore, it is observed from Fig. 5 that the predicted weld pool geometries are in good agreement with the corresponding experimentally observed values.

The similarity in the weld pool geometry observed for samples with 20 and 150 ppm sulfur welded at a laser power of 1900 W can be understood from the velocity and temperature fields presented in Fig. 5A and D. The results show that the peak temperature reached on the weld pool surface for both cases is about 1720 K. The relatively low temperature gradients on the weld pool surface lead to low surface velocities and an insignificant effect of convection on the weld pool geometry. The effect of convection on pool geometry can be examined from the dimensionless Peclet number for heat transfer, Pe . The Peclet number is a measure of the relative magnitudes of convective and conductive heat transfer and is given by:

$$Pe = V_{max}L / \kappa \quad (12)$$

where V_{max} is maximum velocity, κ is the thermal diffusivity of the liquid metal given by $k/\rho C_p$ and L is the characteristic length that can be taken as the depth of the weld pool. Using the data presented in Table 3 and the weld geometries and the maximum surface velocities presented in Fig. 5A to F, the Peclet number can be calculated for various cases. The Peclet numbers for the cases presented in Fig. 5A and D are 0.13 and 0.80, respectively. These low values of $Pe (<1)$ indicate that conductive heat transfer is more important than convective heat transfer in the development of the weld pool geometry in these two cases. As a result, there is no significant difference between the weld pool geometries for steels containing 20 and 150 ppm sulfur for the processing conditions used in this study.

At high laser powers (3850 and 5200 W), the computed Peclet numbers are large (>13). The high Peclet number signifies that the amount of heat transported by convection far outweighs the heat transported by conduction. Therefore, the convective heat transport has a very pronounced effect on the weld pool geometry. For a sulfur content of 20 ppm, dy/dT is negative above 1700 K, as can be observed from Fig. 3B, and therefore, for laser powers of 3850 and 5200 W, negative values of dy/dT prevail over much of the weld pool. In the case of the steel with 20 ppm sulfur, there is only a very small region near the periphery of the weld pool where dy/dT is positive. Except for this small region, the driving force

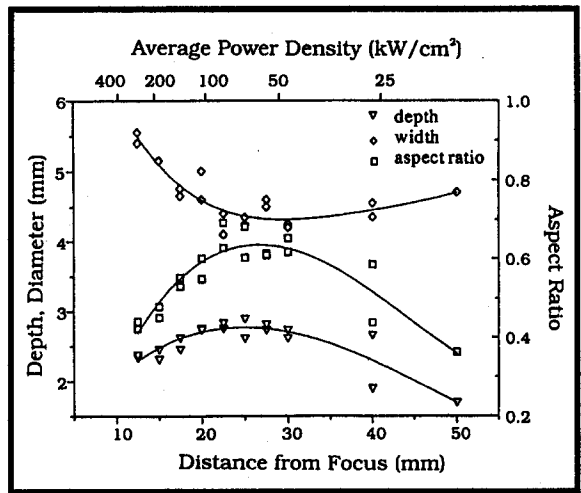


Fig. 6 — Experimental weld pool width, depth and aspect ratio as a function of distance from focus of the laser beam. Laser power 5000 W. Sulfur concentration: 40 ppm. Irradiation time: 15 s.

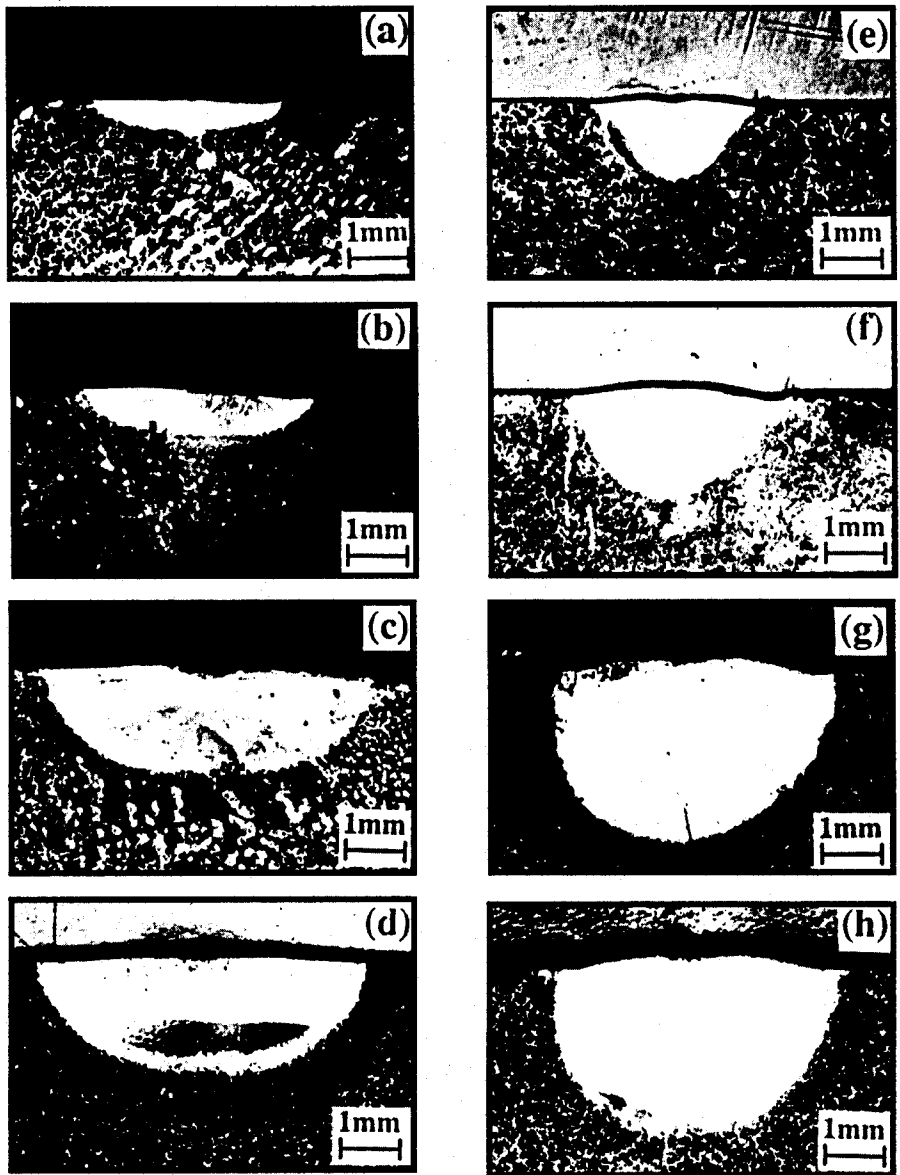


Fig. 7 — Optical micrographs of the weld geometries for the steel containing 20 ppm sulfur for irradiation times of: A — 0.25 s; B — 1 s; C — 10 s; D — 15 s; and for the steel containing 150 ppm sulfur sample for irradiation times of: E — 0.25 s; F — 1 s; G — 10 s; H — 15 s. Laser power: 5200 W.

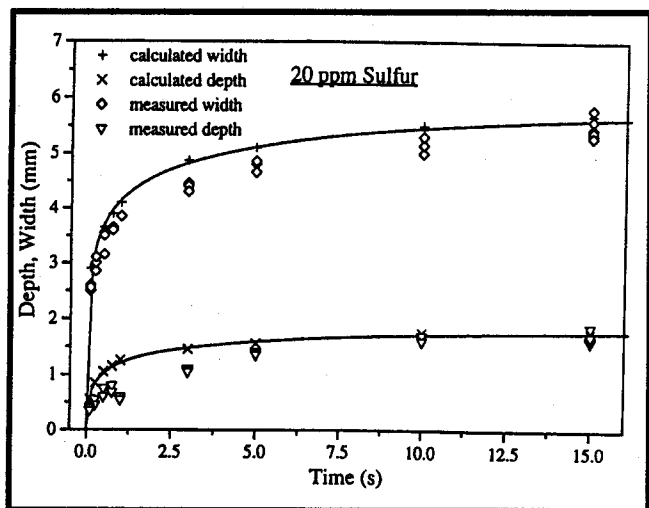


Fig. 8 — Experimental and computed weld pool depth and width as a function of time for the steel containing 20 ppm sulfur. Laser power: 5200 W.

for liquid metal flow in the weld pool is radially outward, *i.e.*, the liquid is transported from the middle of the weld pool to its periphery, as can be observed from Fig. 5B and C. Although the driving force at the pool periphery acts in the opposite direction, it is too weak to drive an inward flow against a strong outward flow near the middle of the surface. Radially outward flow prevails over all of the weld pool surface and results in a shallow weld pool.

When the sulfur content is 150 ppm, the convective heat transport in the

invariant radially inward flow. However, for 5200 W laser power, the peak temperatures are high, and the secondary flow is clearly visible in the velocity field. It will be shown subsequently that opposing flows on the weld pool surface can result in a low aspect ratio under certain conditions of welding.

The heat transfer in the weld pool is affected by the power density of the laser beam. Consequently, the power density affects the temporal development of the weld pool size and aspect ratio. In Fig. 6, the depth, width and aspect ratio of the

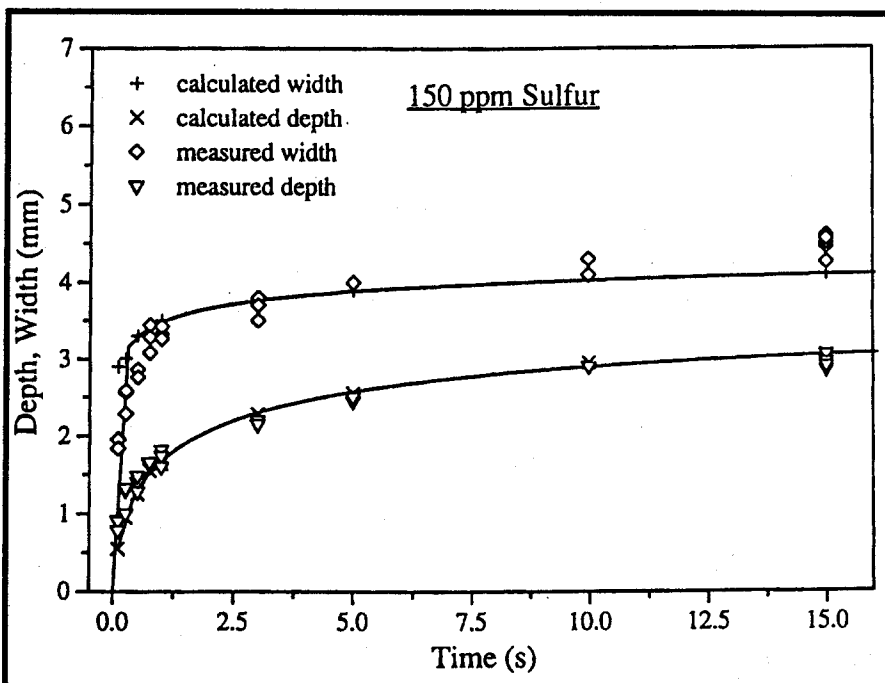


Fig. 9 — Experimental and computed weld pool depth and width as a function of time for the steel containing 150 ppm sulfur. Laser power: 5200 W.

downward direction results in deep pools for both 3850 and 5200 W, as can be observed from Fig. 5E and 5F. Since dy/dT is negative at temperatures higher than 1980 K for the steel containing 150 ppm sulfur, it generates a radially outward secondary flow in a small region near the middle of the pool that opposes the radially inward flow at the pool periphery. At 3850 W, the driving force for this secondary flow is mild and overpowered by the dominant radially inward flow. However, for 5200 W laser power, the peak temperatures are high, and the secondary flow is clearly visible in the velocity field. It will be shown subsequently that opposing flows on the weld pool surface can result in a low aspect ratio under certain conditions of welding.

welds, made on a steel containing 40 ppm sulfur, are plotted as a function of power density, achieved by varying the extent of defocusing of the laser beam when it interacts with the workpiece. The laser power and irradiation time were 5000 W and 15 s, respectively. The results show that the maximum value of aspect ratio is not attained by using either a highly focused or a highly defocused beam. Instead, use of a somewhat defocused beam results in the most favorable aspect ratio under these processing conditions. Thus, the shape of the weld pool can be adjusted, to a certain extent by adjusting the beam power density distribution.

Use of a highly defocused beam leads to relatively low peak temperatures and low thermal gradients on the weld pool surface. As a consequence, the influence of convective heat transfer diminishes when a highly defocused beam is used. On the other hand, when welding with a focused or nearly focused beam, the peak temperatures reached on the weld pool surface are high. As a consequence, when a surface-active element such as sulfur is present in the weld pool, two opposing flows will develop on the weld pool surface (dy/dT is negative below 1785 K for 40 ppm sulfur content in steel). When the radially inward flow is opposed by an equally strong radially outward flow, a high aspect ratio is not attained. It is seen from Fig. 6 that the use of a nearly focused beam results in a relatively low aspect ratio. At moderate defocusing, the temperatures reached on the weld pool surface give rise to positive dy/dT over much of the pool surface resulting in a dominantly inward flow. As a consequence, the resulting weld pool has a high aspect ratio.

In order to examine the temporal evolution of weld pool geometry in steels containing 20 and 150 ppm sulfur, experiments and numerical calculations were carried out for irradiation times of 0.1, 0.25, 0.5, 0.75, 1, 3, 5, 10, and 15 s. The optical micrographs of solidified weld pools after 0.25, 1, 10 and 15 s of laser-material interaction are presented in Fig. 7A to 7H. The micrographs show that for a low-sulfur-content sample, the pool is shallow compared to that for a high-sulfur-content sample at all time steps. The computed results of the time-dependent changes of weld pool depth and width for the sample containing 20 ppm sulfur are presented in Fig. 8. The results show that the predictions of the model are in good agreement with the experimental observations of the pool geometry for different irradiation times. Similarly, the computed results of the

weld pool evolution for the 150 ppm sulfur sample are presented in Fig. 9. Again, the model predictions of weld pool width and depth are in good agreement with the experimental data. Comparison of Figs. 8 and 9 also shows that for the sample containing 150 ppm sulfur, the predicted depth is greater than that for the sample containing 20 ppm sulfur. The temporal evolution of the aspect ratio is shown in Fig. 10. The results indicate that there is a significant increase in the aspect ratio during the first few seconds. This is expected because the depth increases more sharply than the width because of the nature of heat transfer in the weld pool and the geometry of heat flow in the workpiece. The aspect ratio does not change significantly after the initial few seconds in both the steel samples.

The computed pool geometries after 0.5, 5, and 15 s of irradiation of samples containing 20 ppm sulfur are compared with the experimentally observed geometries in Fig. 11A, B and C, respectively. Similar comparisons are made for the sample containing 150 ppm of sulfur in Fig. 12A, B, and C. It is observed from the figures that the computed geometries are in good agreement with the corresponding experimental data. The peak temperature experienced by the pool changes with irradiation time. The changes in the

peak temperature are more rapid in the initial few seconds. Subsequently, the peak temperatures do not change significantly. For example, for the steel containing 20 ppm sulfur, a peak temperature of 2060 K is reached after 0.5 s. However, from 5 s to 15 s, the changes in the peak temperature are insignificant. Furthermore, much of the changes in the fluid flow pattern are established in the initial stages of welding. Since dy/dT is negative above 1700 K for the sample containing 20 ppm sulfur, much of the surface has a negative dy/dT . The negative dy/dT results in an outward flow and the resulting pool is shallow. For the sample with 150 ppm sulfur, the dy/dT shows a different behavior. At the periphery of the pool, the temperatures are low and dy/dT is positive, as can be seen from Fig. 3B. However, in the middle of the weld pool sur-

face, the temperatures are high and dy/dT is negative. As a consequence, the driving force for the fluid flow also changes from radially outward near the middle of the weld pool to radially inward near the periphery, and a complex fluid flow pattern develops in the weld pool. Although the location on the weld pool surface where a change in the direction of shear stress

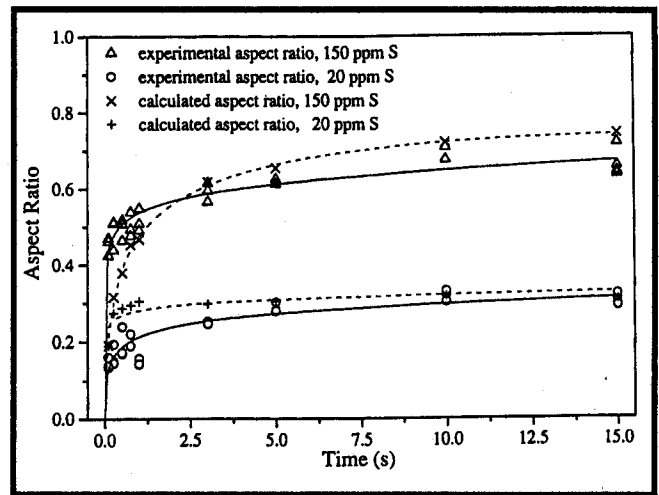


Fig. 10 — Comparison of the experimental and computed aspect ratio at different durations for the steels containing 20 ppm and 150 ppm sulfur. Laser power: 5200 W.

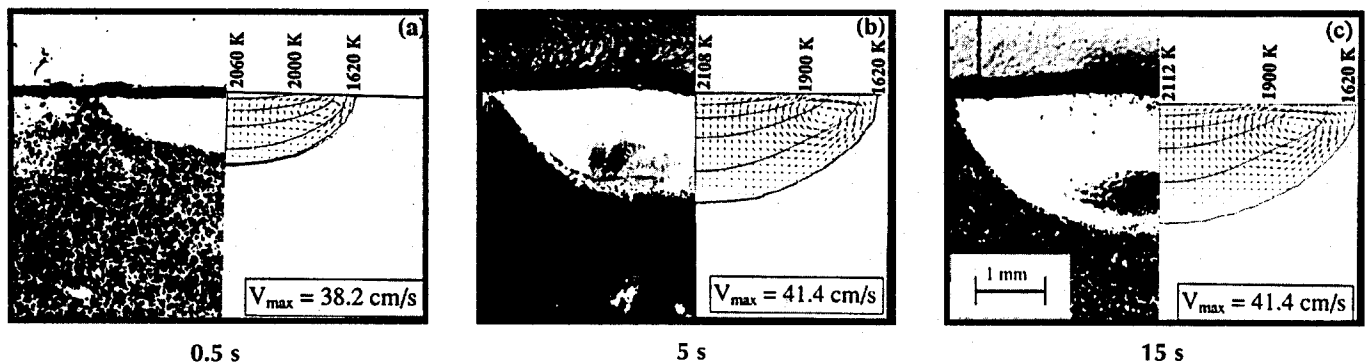


Fig. 11 — Comparison of the computed weld pool geometries with experimental results for irradiation times of 0.5, 5 and 15 s for the steel containing 20 ppm sulfur. Laser power: 5200 W.

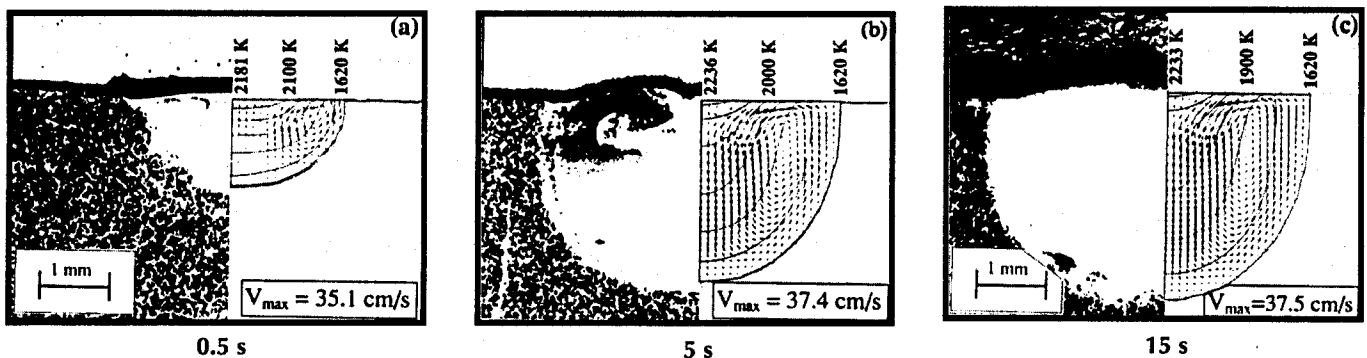


Fig. 12 — Comparison of the computed weld pool geometries with experimental results for irradiation times of 0.5, 5 and 15 s for the steel containing 150 ppm sulfur. Laser Power: 5200 W.

RESEARCH/DEVELOPMENT/RESEARCH/DEVELOPMENT

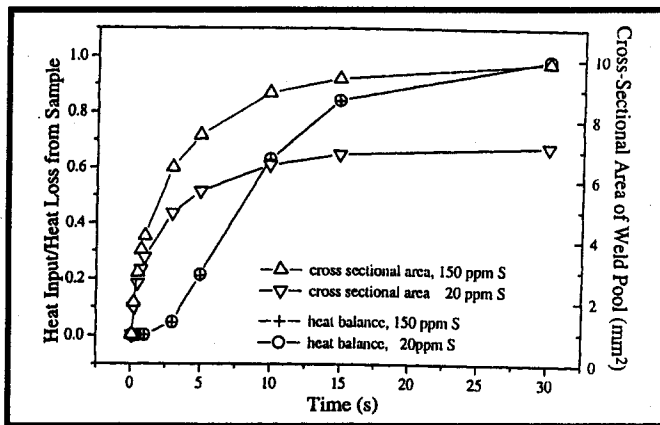


Fig. 13 — Computed cross-sectional area of the weld pool and ratio of heat input to heat loss from the steel samples as a function of time for the steels containing 20 ppm and 150 ppm sulfur. Laser power: 5200 W.

occurs changes with time, the flow is dominantly radially inward. Owing to this flow pattern, heat is transported downward and a deep weld pool is formed. As a consequence of the nature of the convective heat transfer, the temperatures reached on the pool surface are higher in the case of steel with 150 ppm sulfur than those in the case of the steel with 20 ppm sulfur.

The calculated temporal evolution of cross-sectional area of the weld pool is shown in Fig. 13. The evolution of the area is most pronounced in the first few seconds, and a steady state is not reached for welds conducted for less than about 10 seconds. The data in Fig. 13 also show that when the rapid changes in the pool geometry are over after about 10 seconds, accumulation of energy in the workpiece continues and a thermal steady state for the workpiece, *i.e.* a state when the heat input equals heat loss from all sides of the workpiece, is not attained. For the chosen sample geometry and processing conditions, it takes over 20 seconds for attaining an overall thermal steady state in the workpiece. Of course, the computed values of the changes in the time-dependent temperature distribution in the workpiece will depend on the sample geometry, total power, power distribution and other processing parameters. However, the results in Fig. 13 show that the attainment of a thermal steady state in the workpiece is delayed much after the weld pool geometry is essentially fully developed, and the size of the spot weld pools does not increase further with the increase in the irradiation time.

Summary and Conclusions

A comprehensive experimental and modeling investigation was undertaken to understand the temporal evolution of

the weld pool shape and size during high power conduction mode laser spot welding. The role of sulfur in steel, laser power, power density and irradiation time were investigated experimentally using a multikilowatt carbon dioxide laser, and by mathematical modeling through the solution of the equations of conservation of mass and momentum and energy in transient, two-dimensional form.

Although the presence of sulfur can improve weld penetration in many cases, its presence in the weld metal does not always result in high aspect ratio of the weld. Only when convective heat transport is important, *i.e.*, at high Peclet numbers, concentration of sulfur affects both the temporal evolution and the final shape and size of the weld pool. At a given laser power, the weld aspect ratio can be controlled, to a certain extent, by varying the power density. In the range of processing conditions investigated, the temperature profiles, fluid flow, and shape and size of the weld pool change significantly during the first few seconds of the laser material interaction. For the calculations presented here, the weld pool geometry is almost completely developed in about ten seconds, whereas the overall thermal steady state in the workpiece is not attained until about twenty seconds. Heating of the workpiece continues with time much after the weld pool geometry is essentially fully developed. Our current understanding of heat transfer and fluid flow in welding can serve as a basis for improved understanding of the temporal evolution of weld metal shape and size for high power conduction mode welding of steels with different sulfur contents.

Acknowledgments

This work was supported, in part, by the U.S. Department of Energy, Office of Basic Energy Sciences, Division of Materials Science, under grant number DE-FGO284ER45158, and in part by the Austrian Fonds zur Förderung der gewerblichen Forschung, under project number 6/735 and by the Christian Doppler Society. Help from BÖHLER and Linde Gas is appreciated.

References

- David, S. A., and DebRoy, T. 1992. *Science*, Vol. 257, pp. 497-502.
- Oreper, G. M., and Szekely, J. 1984. *Journal of Fluid Mechanics*, Vol. 147, pp. 53-79.
- Chan, C., Mazumder, J., and Chen, M. M. 1984. *Metallurgical Transactions A*, Vol. 15A, pp. 2175-2184.
- Kou, S., and Wang, Y. H. 1986. *Metallurgical Transactions A*, Vol. 17A, pp. 2265-2270.
- Paul, A., and DebRoy, T. 1988. *Metallurgical Transactions B*, Vol. 19B, pp. 851-858.
- Sheng, I. C., and Chen, Y. 1992. Vol. 114(4): 439-449.
- Mills, K. C., and Keene, B. J., 1990. *International Materials Reviews*, Vol. 35(4): 185-216.
- Kreutz, W., and Pirch, N. 1990. *SPIE Proceedings Series*, Vol. 1276, pp. 343-360.
- Matsunawa, A. 1992. *International Trends in Welding Science and Technology*, S. A. David and J. M. Vitek, Eds., ASM International, Materials Park, Ohio, pp. 3-16.
- Choo, R. T. C., Szekeley, J., and David, S. A. 1992. *Metallurgical Transactions B*, Vol. 23B, pp. 371-384.
- Tsotridis, G., Rother, H., and Hondros, E. D. 1989. *Naturwissenschaften*, Vol. 76, pp. 216-218.
- Heiple, C. R., and Roper, J. R. 1982. *Welding Journal* 61(4): 97-s to 102-s.
- Heiple, C. R., and Roper, J. R. 1981. *Welding Journal* 60(8): 143-s to 145-s.
- Heiple, C. R., and Roper, J. R. 1982. *Trends in Welding Research in the United States*, S. A. David, Ed., ASM, Materials Park, Ohio, p. 489.
- Heiple, C. R., Roper, J. R., Stagner, R. T., and Aden, R. J. 1983. *Welding Journal* 62(3): 72-s to 77-s.
- Zacharia, T., David, S. A., Vitek, J. M., and DebRoy, T. 1989. *Welding Journal* 68(12): 499-s to 509-s.
- Zacharia, T., David, S. A., Vitek, J. M., and DebRoy, T. 1989. *Welding Journal* 68(12): 510-s to 519-s.
- Wallner, J. 1964. *Berg- und Hüttenmaennische Monatshefte* 109(3): 107-110 (in German).
- Mundra, K., and DebRoy, T. 1993. Unpublished Research, The Pennsylvania State University, State College, Pa.
- McNallan, M. J., and DebRoy, T., 1991. *Metallurgical Transactions B*, Vol. 22B, pp. 557-560.
- Sahoo, P., DebRoy, T., and McNallan, M. J. 1988. *Metallurgical Transactions B*, Vol. 19, pp. 483-491.